
Thermodynamic and economic analysis of the air source heat pump system with direct-condensation radiant heating panel

Suola Shao^{a, b}, Huan Zhang^{a, b}, Xianwang Fan^{a, b}, Shijun You^{a, b}, Yaran Wang^{a, b*}, Shen Wei^c

^a School of Environmental Science and Engineering, Tianjin University, Haihe Education Area, Jinnan District, Tianjin 300350, PR China

^b Key Laboratory of Efficient Utilization of Low and Medium Grade Energy (Tianjin University), Tianjin 300350, PR China

^c The Bartlett School of Construction and Project Management, University College London (UCL), London WC1E 7HB, United Kingdom

Abstract

The air source heat pump (ASHP) system with the direct-condensation radiant heating panel (DRHP) is an efficient space heating method. To evaluate the energy and exergy efficiencies of the system, a thermodynamic model was established. The effects of external air temperature, indoor air temperature and condensation temperature on the system efficiencies were investigated comprehensively. Results indicate that the low compression ratio is beneficial to the improvement of the energy and exergy efficiency of the system. The efficiency superiority of the system is corroborated in comparison with other ASHP systems. Meanwhile, the economic performances of the system are investigated with the initial cost, operating cost and several economic indicators. To examine the operating cost of the system, a reliable system model is proposed and the

* Corresponding author. Tel.: +8602227892626; fax: +8602227892626.

E-mail addresses: yaran_wang@tju.edu.cn

hourly heating load rates of a case study are presented. Results show that the dynamic investment pay-back period and the internal rate of return of the proposed system are 7.3 years and 11.2%, respectively. The economic competitiveness of the proposed system is demonstrated in comparison with other traditional ASHP heating systems.

Keywords

air-source heat pump; direct-condensation radiant heating panel; thermodynamic analysis; system mathematical model; economic evaluation

Nomenclature	
a	Direct measurements
Bo	Boiling number
C	Cost (USD)
c_p	Specific heat capacity ($\text{kJ kg}^{-1} \text{K}^{-1}$)
d	Diameter of the tube pipe (m)
E	Rate of energy (kW)
e	Fin spacing (m)
Ex	Rate of exergy (kW)
F	Surface area of the evaporator (m)
G	Mass velocity ($\text{kg m}^{-2} \text{s}^{-1}$)
h	Specific enthalpy (kJ kg^{-1})
h_{lh}	Latent heat of vaporization (kJ kg^{-1})
k	Adiabatic exponent
K	Heat transfer coefficient ($\text{W m}^{-2} \text{K}^{-1}$)
m	Flow rate (kg s^{-1})
P	Pressure (bar)
P_q	Water vapor pressure (Pa)
Q	Heating capacity (kW)
R	Fouling resistance ($\text{m}^2 \text{ }^\circ\text{C W}^{-1}$)
Re	Reynolds number
s	Specific entropy ($\text{kJ kg}^{-1} \text{ }^\circ\text{C}^{-1}$)
S	Pipe spacing (m)
T	Temperature ($^\circ\text{C}$)

Nomenclature

u	Velocity (m s^{-1})
W	Electric power consumption (kW)
We	Weber number

Greek symbols

Δ	Variation
α	Convective heat transfer coefficient ($\text{W m}^{-2} \text{K}^{-1}$)
δ	Thickness (m)
η	Compressor efficiency
λ	Thermal conductivity ($\text{W m}^{-1} \text{K}^{-1}$)
μ	Uncertainties
μ_l	Dynamic viscosity of the refrigerant (Pa s)
ζ	Moisture absorption coefficient
ρ	Density (kg m^{-3})
σ	Surface tension (N m^{-1})
v	Velocity at net passage section (m s^{-1})
τ	Annual heating operation hours
φ	Exergy efficiency
ϕ	Heat flux (W m^{-2})

Subscript

0	Dead state
1 ~ 4	State points
Be	Benefit
OC	Operating cost
AC	Annual cost
com	Compressor
con	Condenser
dest	Destruction
dir	Direct
ele	Electric
eva	Evaporator
exa	External air
ICC	Initial capital cost
in	Inlet
ina	Indoor air

Nomenclature

ind	Indirect
LC	Labor cost
ma	Maintenance cost
mp	Market price
no	Nominal condition
oc	Operating cost
out	Outlet
pip	Pipeline
ref	Refrigerant
rev	Reversed
sys	System
VAT	Value-added tax

Acronyms

ASHP	Air source heat pump
<i>COP</i>	Coefficient of performance
DRHP	Direct-condensation radiant heating panel
<i>ic</i>	Influence coefficient
<i>IRR</i>	Internal rate of return
<i>NPV</i>	Net present value
<i>P_t</i>	Dynamic investment pay-back period

1. Introduction

In 2018, global energy consumption increased by 2.3% [1], 36% of which was used for space heating and cooling in buildings [2]. Creating a comfortable indoor environment through low-cost and electrified clean energy technology is considered as an effective countermeasure for energy conservation [3]. As a clean and sustainable heating technology, the ASHP system has been widely utilized in areas without district heating.

The ASHP system can be categorized into ASHP air-to-water heating system and ASHP refrigerant-to-air heating system [4]. Compared with other traditional heating measures, the ASHP air-to-water heating system reduces energy consumption by 36% [5]. Shan et al. [6] integrated solar energy to the ASHP air-to-water heating system to increase the system *COP*. Gang et al. [7] proposed an instantaneous heating mode for the air-to-water system and found that the *COP* was 24% higher than that in the cyclic heating mode. However, due to the secondary heat transfer in the water heating cycle, the efficiency of the air-to-water heating system is degraded [8]. In the ASHP refrigerant-to-air heating system, the split air conditioner is one of the most common heating terminals. The system *COP* changes from 2 to 4 when the external air temperature varies between $-15\text{ }^{\circ}\text{C}$ and $+7\text{ }^{\circ}\text{C}$ in the tests of Christensen et al. [9], which is higher than that in the air-to-water heating system [10]. However, Lin et al. [11] found that the forced convection caused by fans of the split air conditioner will lead to discomfort. Meanwhile, the indoor air velocity distribution was more chaotic in the heating system with fans [12].

The heat loss in the air-to-water heating system and the indoor discomfort brought by the fan in the refrigerant-to-air heating system promote the emergence of fan-less direct-condensation heating terminals, which rely on natural convection and radiation for space heating [13]. The ASHP system with the direct-condensation floor was studied by Dong et al. [14] and Ma et al. [15]. The *COP* of the system was 2.05 at the external air temperature of $-15\text{ }^{\circ}\text{C}$ [14] and the indoor temperature field met the requirements in

ASHRAE 55-2004 [15,16]. In the authors' previous study [17], a direct-condensation heating terminal was proposed for the ASHP system. The system was proved to be reliable with comfortable indoor thermal in heating conditions.

Apart from the thermal performances of the ASHP system, the energy and exergy efficiencies are important indicators of the system's thermodynamic performance [18]. For different ASHP heating systems, the energy and exergy destructions of components are different [19]. As pointed out by Kilkis [20], the key factor to determine the success of the HP system is whether the energy and exergy are matched with the demand of the heating terminals. However, there is little research on the thermodynamic performances of the ASHP system with the direct-condensation heating terminal.

In this paper, the thermal stability, energy and exergy efficiencies and the economic performances of the air source heat pump (ASHP) system with a direct-condensation radiant heating panel (DRHP) were examined. To explore the energy and exergy utilization of the ASHP system with the DRHP, a thermodynamic model was established. The effects of external air temperature, indoor air temperature and condensation temperature on the system utilization rate were discussed comprehensively. Meanwhile, the efficiency of the presented system was compared with other traditional ASHP systems to verify efficiency superiority. To investigate the system economy, the initial cost, operating cost and economic evaluation indicators of the system were analyzed. The mathematical model of the proposed system was established and the hourly heating load rates of a case study were presented to estimate

the system operating cost. The economic competitiveness of the system was demonstrated in comparison with other heating systems.

2. Experimental setup

Experiments were conducted based on EN 442-2-2014 [21]. As shown in Fig. 1, a standard-compliant calorimetric chamber, consisting of indoor and outdoor compartments with a size of 4 m (L) × 4 m (W) × 3 m (H) is the experimental site. Both compartments were equipped with independent air-conditioning systems. To guarantee the indoor flow field, a chamber of 3.5 m (L) × 3.5 m (W) × 2.5 m (H) was built in the indoor compartments to avoid forced convection from the indoor air-conditioning system.



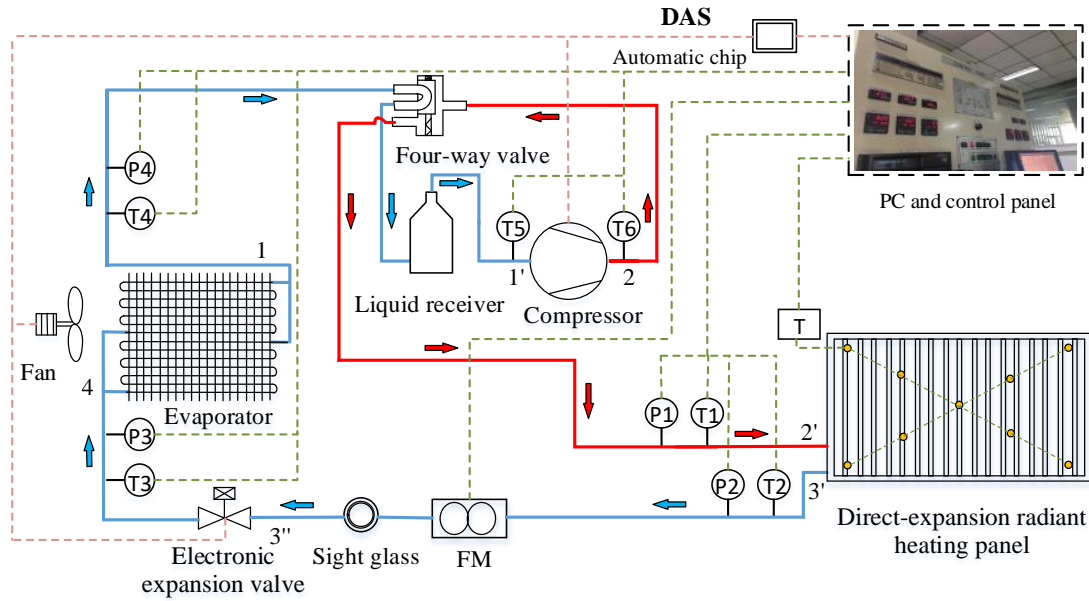
Fig. 1. The prototype of the calorimetric chamber.

2.1 System description

The ASHP system with the DRHP and the data acquisition system (DAS) are illustrated in Fig. 2. The heating system consists of a DRHP, an electronic expansion valve (EEV), an outdoor heat exchanger, a liquid receiver, a four-way valve, and a rotary compressor. The structure diagram of the DRHP is depicted in Fig. 3. Water is selected as heat storage material to fill the gaps in the DRHP. The details of the system are shown in Table. 1.

Table. 1. Information on the components of the proposed system.

Components	Information
Compressor	Type: hermetic motor compressor with twin rotary; Nominal heating capacity:12000 Btu/h; Displacement: 10.2 cm ³ /rev
Direct-condensation radiant heating panel	Dimension: 0.9 m × 0.08 m × 1.6 m (L × W × H); Single panels; 48 vertical channels; 39 m copper tube; 3.26 kg water; 48 sets of ribs
Electronic expansion valve	Type: DPF(Q)1.8 Size: 717 mm×483 mm×230 mm; 3 paths;
Outdoor heat exchanger	Copper pipe: length of 30.8 m, external diameter of 7 mm (inner diameter of 6 mm); Pipe spacing: 25 mm; Fin thickness: 0.1 mm; Fin spacing:1.8 mm
Refrigerant	Type: R410A; Charge: 0.80 kg



T1/P1 inlet temperature/pressure of DRHP
 T2/P2 outlet temperature/pressure of DRHP
 T3/P3 inlet temperature/pressure of evaporator
 T4/P4 outlet temperature/pressure of evaporator
 T5/T6 suction/ discharge temperature of the compressor
 T temperatures arranged in the DRHP

Fig. 2. The ASHP system with the DRHP.

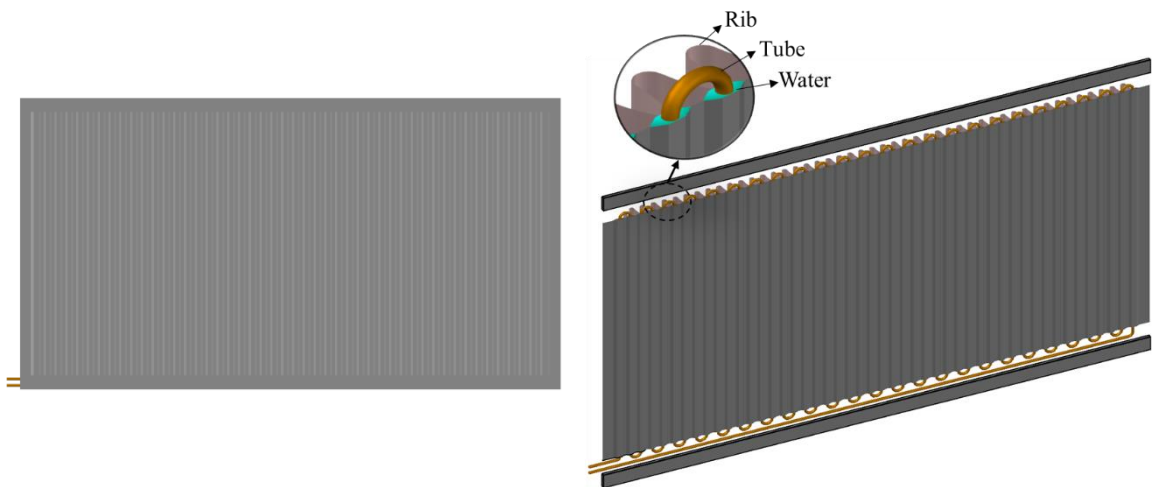


Fig. 3. The structure diagram of the DRHP.

2.2 Experimental control strategy

The external and indoor air parameters can be regulated with the air-conditioning systems of the calorimetric chamber. The external air relative humidity (RH) changes from 40% to 88%. The external air temperature (T_{exa}) changes from $-10\text{ }^{\circ}\text{C}$ to $12\text{ }^{\circ}\text{C}$

while the indoor air temperature (T_{ina}) changes from 16 °C to 24 °C in experiments. Meanwhile, the condensation pressure of the heating system is controlled via the adjustment of the compressor frequency, the outdoor fan speed, and the opening of the EEV. The control commands are set in an automatic chip associated with the control panel. Through the control panel, the air-conditioning systems of the calorimetric chamber and the automatic chip of the proposed system can be adjusted synchronously.

2.3 Measurements and uncertainty analysis

Based on the Chinese Standard JG/T 403-2013 [22], the following parameters are measurements.

- (a) The refrigerant flow rates are tested by Coriolis Mass Flowmeter.
- (b) The compressor input power is calculated by a wattmeter.
- (c) The condensation and evaporation pressures are tested by Pressure Transmitters.
- (d) The temperatures and RH are measured by copper-constantan thermocouples and Testo.

The uncertainties resulting from the limited precision of the measuring instruments are calculated according to the method from Ref. [23] and Ref. [24]. The uncertainty of temperature, pressure and flow rate [23] is:

$$\mu_{\text{dir}} = \sqrt{\frac{1}{n-1} \sum_{i=1}^n (a_i - \frac{1}{n} \sum_{i=1}^n a_i)^2} \quad (1)$$

where a represents the direct measurements, and n is the measuring times.

The uncertainties of the system COP and the heating capacity of the DRHP are associated with the random error (μ_i) of the direct measurements, and the relation is formulated as [24]:

$$\mu_{ind} = \sqrt{\sum_{i=1}^n \left(\frac{\partial f}{\partial a_i} u_i \right)^2} \quad (2)$$

The measurements and the uncertainties are shown in Table. 2.

Table. 2. The experimental range of measurements.

Measured parameters	Experimental range	Accuracy	Error range (%)
T	14 °C ~ 72 °C	±0.5 °C	±0.69 ~ 3.57
RH	40%~88%	±2%	±2.27 ~ 5.00
P	4.6 bar ~ 22.8 bar	0.1%FS	±0.10
m	35.5 kg/h ~ 64 kg/h	±0.002 kg/h	±0.003 ~ 0.006
W	0.46 kW ~ 1.46 kW	±0.01 kW	±0.69 ~ 2.17
Q_{con}	1.70 kW ~ 2.72 kW	/	±0.48 ~ 0.97
COP	1.79 ~ 4.45	/	±0.91 ~ 5.68

3. Methodology

3.1 Thermodynamic model

To analyze the thermodynamic performance of the ASHP system with the DRHP, the lg p - h diagram is illustrated in Fig. 4. The physical locations of the corresponding cycle point 1~ 4 are annotated in Fig. 2. For simplicity, the following assumptions are considered:

- (a) The refrigerant keeps a steady state without any chemical reactions.
- (b) The throttling processes are isenthalpic (i.e. $h_3 = h_4$).
- (c) The outdoor environment is considered as the dead state for the proposed

system [25].

- (d) The input power of the outdoor fans is negligible compared with that of the compressor.
- (e) The heat loss and exergy destruction in the pipeline 1-1' and 3'-3'' are ignored for the small temperature drop.
- (f) The evaporation and condensation pressure involved in the paper is unified as the average pressure of the import and export parts.

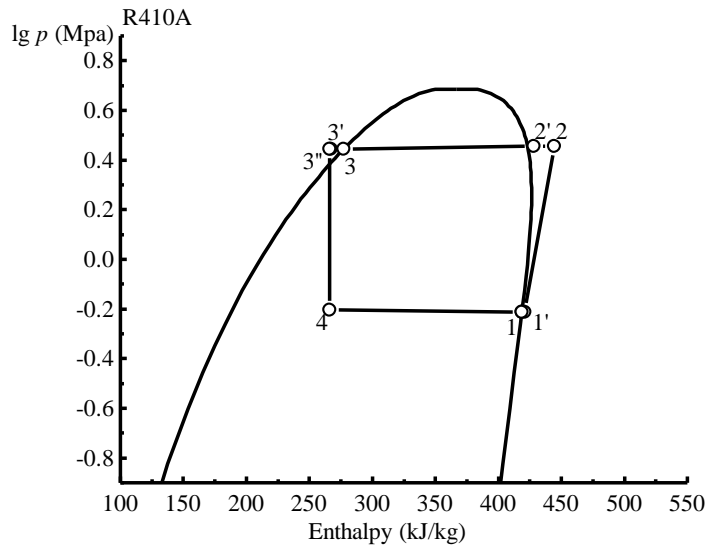


Fig. 4. $\lg p$ - h diagram of the ASHP system with the DRHP.

3.1.1. Energy analysis

The energy rate and energy efficiency of the system are discussed. The mass balance and heat balance are expressed as:

$$\sum m_{in} = \sum m_{out} \quad (3)$$

$$\sum E_{in} = \sum E_{out} \quad (4)$$

The energy balance equation of each component of the system can be expressed

as follows,

for the condenser (DRHP),

$$mh_{2'} = Q_{\text{con}} + mh_3 \quad (5)$$

for the EEV,

$$mh_{3''} = mh_4 \quad (6)$$

for the evaporator,

$$mh_4 + Q_{\text{eva}} = mh_1 \quad (7)$$

$$Q_{\text{eva}} = Q_{\text{fan}} \quad (8)$$

for the compressor,

$$mh_1 + W = mh_2 \quad (9)$$

The heat loss and exergy destruction in the pipeline 2-2' are taken into account due to its significant temperature drop. The heat emission of the system Q_{sys} equals the sum of the energy rate of the DRHP and the heat loss of the pipeline 2-2'.

$$Q_{\text{sys}} = Q_{\text{con}} + Q_{\text{pipeline2-2'}} \quad (10)$$

$$Q_{\text{pipeline2-2'}} = mh_2 - mh_{2'} \quad (11)$$

The energy conservation of the system is given as follows:

$$COP = \frac{Q_{\text{con}}}{W} \quad (12)$$

3.1.2. Exergy analysis

The exergy balance equation of the fluid in the steady-flow process is:

$$Ex_{\text{in}} - Ex_{\text{out}} = Ex_{\text{dest}} \quad (13)$$

which can be further subdivided into:

$$Ex_{\text{heat}} - Ex_{\text{work}} + Ex_{\text{mass,in}} - Ex_{\text{mass,out}} = Ex_{\text{dest}} \quad (14)$$

The flow exergy rate Ex_{mass} and the exergy transfer rate of heat and work (Ex_{heat} and Ex_{work}) are defined as follow:

$$Ex_{\text{mass,in}} = \sum m_{\text{in}} [(h_{\text{in}} - h_0) - T_0 (s_{\text{in}} - s_0)] \quad (15)$$

$$Ex_{\text{mass,out}} = \sum m_{\text{out}} [(h_{\text{out}} - h_0) - T_0 (s_{\text{out}} - s_0)] \quad (16)$$

$$Ex_{\text{heat}} = \sum (1 - \frac{T_0}{T_n}) Q_n \quad (17)$$

$$Ex_{\text{work}} = W \quad (18)$$

The exergy efficiency of the system, φ employed here is defined with the thermodynamic model in Refs. [26], which can also be expressed by the coefficients of performance [27]:

$$\varphi = \frac{\text{Exergy recovered}}{\text{Exergy supplied}} = \frac{\sum (1 - \frac{T_0}{T_n}) Q_n}{W} = \frac{COP}{COP_{\text{HP,rev}}} \quad (19)$$

$$COP_{\text{HP,rev}} = \frac{1}{1 - T_0 / T_{\text{ina}}} \quad (20)$$

where $COP_{\text{HP,rev}}$ is the coefficient of performance in reversed Carnot cycle.

The task efficiency, a ratio between COP and the ideal Carnot heat pump performance between the equivalent evaporation temperature and equivalent condensation temperature ($COP_{\text{HP,rev-euq}}$), is used to examine the proposed system performance.

$$\eta = \frac{COP}{COP_{\text{HP,rev-euq}}} \quad (21)$$

$$COP_{\text{HP,rev-euq}} = \frac{1}{1 - T_{\text{eva}} / T_{\text{con}}} \quad (22)$$

The exergy transfer diagrams of the system components and the exergy equations

are shown in Table. 3. It should be emphasized that the refrigerant absorbs the heat energy of external air in the evaporator. Based on the definition of exergy, the exergy value of external air is 0 [28].

Table 3. Exergy rate balance equations of the system's components.

Component	Exergy transfer diagram	Exergy rate balance equation	Exergy efficiency
Direct- condensation radiant heating panel		$Ex_{\text{dest,con}} = m[(h_{2'} - h_{3'}) - T_0(s_{2'} - s_{3'})]$ $- Q_{\text{con}} \left(1 - \frac{T_0}{T_{\text{ina}}}\right)$	$\varphi_{\text{con}} = \frac{Q_{\text{con}} \left(1 - \frac{T_0}{T_{\text{ina}}}\right)}{m[(h_{2'} - h_{3'}) - T_0(s_{2'} - s_{3'})]}$
Electronic expansion valve		$Ex_{\text{dest,EEV}} = m[(h_{3''} - h_4) - T_0(s_{3''} - s_4)]$	$\varphi_{\text{EEV}} = \frac{(h_4 - h_0) - T_0(s_4 - s_0)}{(h_{3''} - h_0) - T_0(s_{3''} - s_0)}$
Outdoor heat exchanger		$Ex_{\text{dest,eva}} = m[(h_4 - h_1) - T_0(s_4 - s_1)] + Ex_{\text{heat,eva}}$ $= m[(h_4 - h_1) - T_0(s_4 - s_1)]$ $Ex_{\text{heat,eva}} = 0$	$\varphi_{\text{eva}} = \frac{(h_1 - h_0) - T_0(s_1 - s_0)}{(h_4 - h_0) - T_0(s_4 - s_0)}$
Compressor		$Ex_{\text{dest,com}} = W + m[(h_{1'} - h_2) - T_0(s_{1'} - s_2)]$	$\varphi_{\text{com}} = \frac{m[(h_2 - h_{1'}) - T_0(s_2 - s_{1'})]}{W}$

The exergy destruction of the system pipeline 2-2' is as follows:

$$Ex_{\text{dest,pip}} = m[(h_2 - h_{2'}) - T_0(s_2 - s_{2'})] \quad (23)$$

The involved numbers are shown in Fig. 2 and 4, and the relevant characters can be found in the Nomenclature Table.

3.2. Economic model

The initial capital cost (C_{ICC}) and annual operating cost (C_{OC}) are investigated in the system economic model. To further evaluate the economic performances, the economic indicators, such as the total annual cost (C_{AC}), dynamic investment pay-back period (P^t), the net present value (NPV) and the internal rate of return (IRR), are also taken into consideration.

3.2.1 System initial investment

The initial capital cost (C_{ICC}) is composed of the market price of the components (C_{mp}), the value-added tax (C_{VAT}), and the labor cost (C_{LC}), which can be expressed as follows:

$$C_{\text{ICC}} = C_{\text{mp}} + C_{\text{VAT}} + C_{\text{LC}} \quad (24)$$

where C_{mp} consists of the cost of the compressor (C_{com}), the cost of the evaporator (C_{eva}), the cost of the DRHP (C_{DRHP}), and the cost of accessories (C_{add}). C_{VAT} of each component is determined by Ref.29, and C_{LC} of the system is considered to be 5% of C_{ICC} .

3.2.2 Operating cost

The annual operating cost (C_{OC}) of the proposed system depends on the building heating load and the heat transfer characteristics of the system loop [30]. The expression of C_{OC} is given as:

$$C_{OC} = \sum W \times C_{ele} \times \tau \quad (25)$$

where $\sum W$ represents the total input power of the compressor from Nov 15th to Mar 15th in the typical meteorological year [31], while the electricity price (C_{ele}) equals 0.073 \$/kWh [32].

3.2.2.1 Mathematical model of the heat pump system

The heat transfer characteristics of the system loop could be obtained through the mathematical model of the ASHP system with the DRHP.

For the condenser (DRHP), the energy balance equation of the refrigerant at the DRHP is expressed as follows:

$$Q_{con} = m(h_{2'} - h_{3'}) \quad (26)$$

where the point of 2' can be inferred from the heat loss of the pipeline 2-2', which is examined in this paper, and the point of 3' can be obtained from the degree of supercooled, which changes around 5 ± 1.5 °C in experiments.

Meanwhile, the heat transfer model of the DRHP is proposed in the authors' previous work [33]. Referring to the DRHP model, the heat transfer characteristics of the DRHP under different heating conditions are available. Accordingly, through the collection of DRHP model data, the relationship between DRHP heating capacity and

different operating parameters can be obtained.

For the evaporator, the heat transfer model is established based on the following assumptions:

- (1) The heat transfer process is steady-state;
- (2) The contact thermal resistance and pressure drop of the evaporator are ignored;
- (3) The effects of frosting are ignored in the evaporator model. However, to ensure the practicability of the system model, the simulation data are modified with the influence coefficients (*ic*) of frost conditions on system performance in Ref. 34.

The energy balance equations of the evaporator model are given as follows:

- (1) The energy balance equation of the refrigerant:

$$Q_{\text{eva}} = m(h_1 - h_4) \quad (27)$$

- (2) The energy balance equation of the ambient air:

$$Q_{\text{air}} = m_{\text{air}} c_p (T_{\text{air-in}} - T_{\text{air-out}}) \quad (28)$$

where the m_{air} is the velocity, c_p is the specific heat capacity, $T_{\text{air-in}}$ is the inlet air temperature (i.e. T_{exa}) while $T_{\text{air-out}}$ is the outlet air temperature.

- (3) The heat transfer between refrigerant fluid and the ambient air:

$$Q_{\text{heat,eva-air}} = KF \left(\frac{T_{\text{air-in}} - T_{\text{air-out}}}{\ln \frac{T_{\text{air-in}} - T_{\text{eva}}}{T_{\text{air-out}} - T_{\text{eva}}}} \right) \quad (29)$$

where the T_{eva} is the evaporation temperature, F is the surface area of the evaporator.

K is the overall heat transfer coefficient of the evaporator, given as follows [35]:

$$K = \frac{1}{\frac{A_{\text{out}}}{\alpha_{\text{out}} (A_{\text{pipe-out}} + \eta A_{\text{fin}}) \xi} + \frac{\delta_{\text{pipe}}}{\lambda_{\text{pipe}}} \frac{A_{\text{out}}}{A_{\text{in}}} + R_{\text{out}} + \frac{1}{\alpha_{\text{in}}} \frac{A_{\text{out}}}{A_{\text{in}}}} \quad (30)$$

$$\xi = \frac{h_{\text{air-in}} - h_{\text{air-out}}}{c_p (T_{\text{air-in}} - T_{\text{air-out}})} \quad (31)$$

$$h_{\text{air}} = 1.005T_{\text{air}} + (2500 + 1.84T_{\text{air}}) \frac{0.622P_q}{P - P_q} \quad (32)$$

where ξ is the moisture absorption coefficient, which represents the latent heat transfer of evaporator [36], P_q is the water vapor pressure, α_{out} and α_{in} are the convective heat transfer coefficient between the evaporator and ambient air, between the refrigerant and the copper pipe, A_{out} , $A_{\text{pipe-out}}$, A_{in} , and A_{fin} are the surface area of the finned tube, the outside area of copper pipes, the inside area of copper pipes, and the area of fins. δ_{pipe} and λ_{pipe} are the thickness and thermal conductivity of the copper pipe. R_{out} is the fouling resistance of the evaporator, which is $2.8 \times 10^{-4} \text{ m}^2 \text{ }^\circ\text{C/W}$ [37].

The heat transfer intensity between the forked finned bundles and ambient air is expressed as [38]:

$$\alpha_{\text{out}} = 18\nu^{0.578} \quad (33)$$

$$\nu = u_{\text{air}} / \varepsilon \quad (34)$$

$$\varepsilon = \frac{(S - d_{\text{out}})(e - \delta_{\text{fin}})}{S \times e} \quad (35)$$

where ν is the air velocity at net passage section, u is air velocity, which is 1.8 m/s at the fan speed of 650 r/s, S is the pipe spacing, e is the fin spacing, and d_{out} is the outer diameter of the pipe.

The heat transfer coefficient α_{in} is determined by Sun and Mishima [39]:

$$\alpha_{in} = \frac{6 Re_1^{1.05} Bo^{0.54} \lambda_1}{We_1^{0.191} (\rho_1 / \rho_g)^{0.142} d_{in}} \quad (36)$$

$$Re_1 = \frac{G d_{in}}{\mu_1} \quad (37)$$

$$Bo = \frac{\phi}{G h_{lh}} \quad (38)$$

$$We_1 = \frac{G^2 d_{in}}{\sigma \rho_1} \quad (39)$$

where Re_1 is the Reynolds number, Bo is the Boiling number, We is the Weber number, μ_1 is the dynamic viscosity of the refrigerant, G is the mass velocity, ϕ is the heat flux, h_{lh} is the latent heat of vaporization, σ is the surface tension of the refrigerant, ρ_1 and ρ_g are the density of the refrigerant liquid and refrigerant gas.

For the compressor, the exhaust temperature of the compressor is given as follows:

$$T_2 = T_1 \left(\frac{P_2}{P_1} \right)^{\frac{k-1}{k}} \quad (40)$$

where T_1 is the suction temperature, equals T_{eva} , T_2 is the exhaust temperature, P_1 and P_2 are the evaporation and condensation pressures, k is the adiabatic exponent obtained from the manufacturer.

The input power of the compressor is defined as follows:

$$P_{in} = \frac{m(h_2 - h_1)}{\eta_i \eta_m \eta_d \eta_e} \quad (41)$$

$$\eta_i = 1 - 0.6 \left[1 - \left(\frac{P_2}{P_1} \right)^{-0.3} \right] \quad (42)$$

where η_i is the indicated efficiency, η_m is the friction efficiency, η_d is the transmission efficiency and the value is 1, η_e is the shaft efficiency and the value is 0.78 [38].

The mathematical model of the system is established with Eq. 26~Eq. 42. Considering the effects of frosting on the mathematical model, the modified method followed by Zhu et. al [34] and Liu et. al [40] is applied to the simulation data. As shown in Fig. 5, the frosting region zone is divided into five regions. The influence coefficients (ic) of the five regions on the system COP are shown in Table. 4. The modified simulated COP_{re} is defined as:

$$COP_{re} = COP \times ic \quad (43)$$

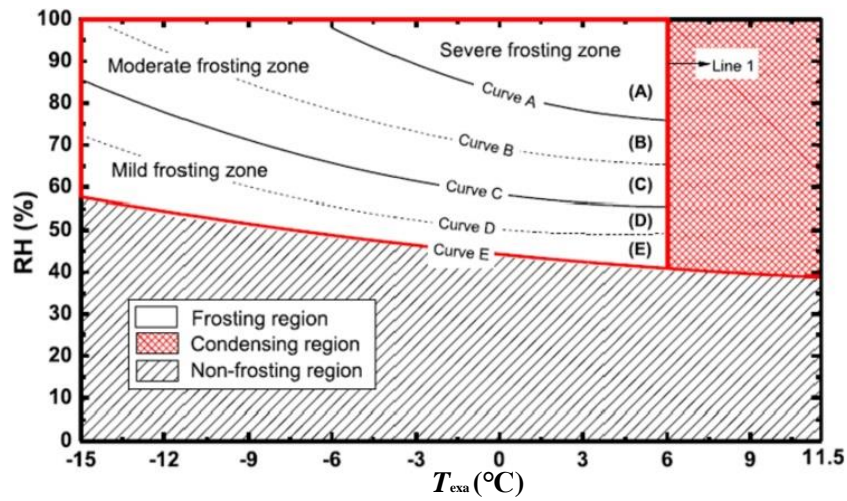


Fig. 5. Frosting map under different external air parameters (Zhu et al., 2015).

Table. 4. The influence coefficients on system performances.

Frosting region	Judgment	ic
A	$0.1186T_{exa}^2 - 1.7874T_{exa} + 82.979 \leq RH < 0.0186T_{exa}^2 - 0.6003T_{exa} + 44.246$	0.68
B	$0.0695T_{exa}^2 - 1.0969T_{exa} + 68.83 \leq RH < 0.1186T_{exa}^2 - 1.7874T_{exa} + 82.979$	0.74
C	$0.0659T_{exa}^2 - 0.8392T_{exa} + 58.349 \leq RH < 0.0695T_{exa}^2 - 1.0969T_{exa} + 68.83$	0.80
D	$0.06T_{exa}^2 - 0.5457T_{exa} + 50.415 \leq RH < 0.0659T_{exa}^2 - 0.8392T_{exa} + 58.349$	0.86
E	$0.0186T_{exa}^2 - 0.6003T_{exa} + 44.246 \leq RH < 0.06T_{exa}^2 - 0.5457T_{exa} + 50.415$	0.89

The flow chart of the mathematical model is as follows:

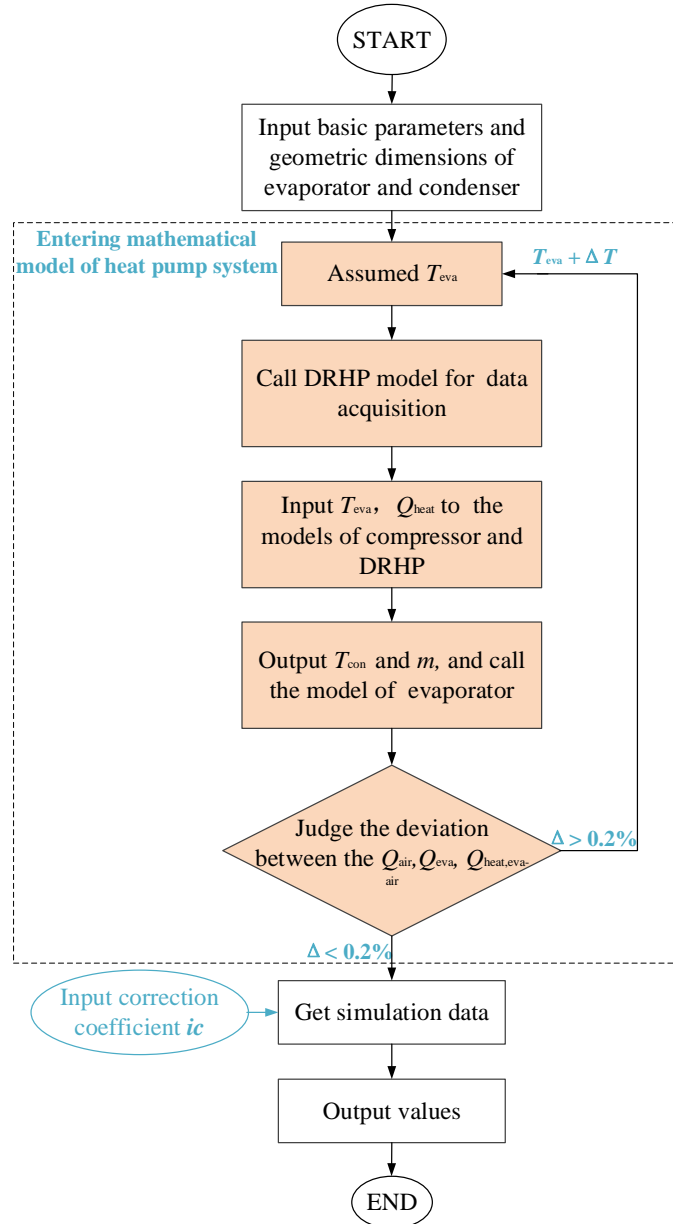


Fig. 6. Flow chart of the mathematical model.

The calculation process of the model is divided into five steps: (1) Input heating load demand and basic parameters of the system, (2) Assume T_{eva} and call the system model to solve the mass flow rate (m) and the condensation temperature (T_{con}), (3) Judge the deviation of the Q_{air} , Q_{eva} , $Q_{heat,eva-air}$, (4) Modify T_{eva} until the deviation meets the requirement, (5) Introduce the influence coefficients of the defrosting condition to the simulation data.

3.2.2.2 Validation of the mathematical model

The feasibility of the system model is demonstrated by comparing the simulation and experimental results. As shown in Table. 5, the experimental heating capacity of the DRHP, T_{exa} and RH are input parameters. The deviation of T_{eva} between the numerical and experimental data changes from -1.0 °C to 0.7 °C, with an absolute mean deviation of 0.5 °C. Moreover, the deviations of T_{con} , m and W are all examined, ranging from -2.9% to 9.8% , -6.7% to 1.6% , and -11.6% to 9.6% , respectively, which are within the acceptable range.

Table. 5. Comparison of the numerical and experimental data of the heat pump system.

Case	1	2	3	4	5	6	7	8	9	
T_{exa} (°C)	-7	-7	-7	-7	-10	-5	5	7	10	
RH (%)	48%	50%	49%	46%	55%	44%	71%	86%	76%	
Q_{heat} (W)	1932	2115	2317	2580	2072	2106	2229	2186	2256	
T_{eva} (°C)	Exp	-9.5	-9.4	-9.3	-9.1	-12.2	-7.5	1.9	3.7	6.4
	Num	-9.2	-9.3	-9.50	-9.7	-12.3	-7.3	2.50	4.6	7.4
	DEV (°C)	-0.3	-0.1	0.2	0.7	0.14	-0.2	-0.6	-0.9	-1.0
T_{con} (°C)	Exp	42.5	46.6	50.9	55.5	46.4	46.1	46.1	46.0	46.6
	Num	43.7	46.1	48.8	52.3	45.5	46.0	47.3	46.6	42.0
	DEV (%)	-2.9	0.9	4.1	5.8	1.9	0.3	-2.6	-1.2	9.8
G (kg/h)	Exp	41.7	47.2	52.69	58.6	46.3	46.5	49.8	49.3	50.4
	Num	42.8	47.4	52.68	59.9	45.6	47.6	53.3	52.5	53.2
	DEV (%)	-2.6	-0.5	0.03	-2.2	1.56	-2.4	-7.0	-6.4	-5.5
W (kW)	Exp	0.73	0.89	1.10	1.38	0.97	0.82	0.64	0.60	0.55
	Num	0.81	0.95	1.11	1.35	1.00	0.89	0.70	0.62	0.50
	DEV (%)	-11.6	-6.6	-1.3	2.2	-3.3	-8.1	-8.9	-3.8	9.6

Note:

Case 2 is the typical heating condition in experiments.

Based on the established mathematical model, the operating cost of the system for space heating could be obtained when the building dynamic heating load is available.

3.2.3 Economic indicators

The total annual cost (C_{AC}) related to C_{ICC} and C_{OC} is calculated as [41]:

$$C_{AC} = C_{ICC} \left[\frac{i(i+1)^n}{(i+1)^n - 1} \right] + C_{OC} + C_{ma} \quad (44)$$

$$C_{ma} = 0.12 \times C_{ICC} \times \left[\frac{i(i+1)^n}{(i+1)^n - 1} \right] \quad (45)$$

where C_{ma} is the maintenance cost, n is the lifetime of the heating system, and the value is 10 years, i is the annual interest rate, and the value is 8%.

The dynamic investment pay-back period (P^t) of the system associated with C_{AC} and the annual benefit (C_{Be}), is defined as follows [42-43]:

$$P^t = t \quad \left[\sum_{t=2}^n (C_{Be} - C_{AC}) - C_{ICC} \right] > 0 \quad + \frac{[C_{ICC} / (1+i) - \sum_{t=2}^n (C_{Be} - C_{AC}) / (1+i)^t]}{(C_{Be} - C_{AC}) / (1+i)^{t+1}} \quad (46)$$

$$C_{Be} = C_{basic,heat} \times A + C_{heat} \times Q_{heat} \quad (47)$$

where Q_{heat} is the total heating load, $C_{basic,heat}$ and C_{heat} are the basic cost associated with the heating area and the heating cost, the values are 2.75 \$/m² and 0.055 \$/kWh in China.

The net present value (NPV) of the proposed system during the whole lifetime is calculated as follows:

$$NPV = \sum_{t=2}^n (C_{Be} - C_{AC}) / (1+i)^t - C_{ICC} / (1+i) \quad (48)$$

The interest rate that makes the project inflows equal to the outflows is defined as the internal rate of return (IRR):

$$\sum_{t=2}^n (C_{Be} - C_{AC-IRR}) / (1+IRR)^t - C_{ICC} / (1+IRR) = 0 \quad (49)$$

If $IRR > i$, the proposed system is profitable, otherwise, the system has no

investment prospects.

4. Results and discussions

4.1 Thermal stability of the system

The operating characteristics of the system are shown in Fig. 7. As shown in Fig.7, the fluctuations of the temperature parameters are faint in the steady stage. The condensation temperature (T_{con}) fluctuates around 46.5 ± 0.1 °C while the T_{eva} fluctuates around -9.4 ± 0.1 °C in the typical heating condition. The superheat of the inlet refrigerant is maintained at 2.7 ± 0.2 °C. Apart from temperature parameters, the refrigerant flow rate of the system oscillates between 47.05 kg/h and 47.37 kg/h with an average value of 47.2 kg/h. Compared with the fluctuations of other HP systems [44, 45], the oscillation amplitude of the proposed system is smaller, demonstrating the stability and reliability of the ASHP system with DRHP.

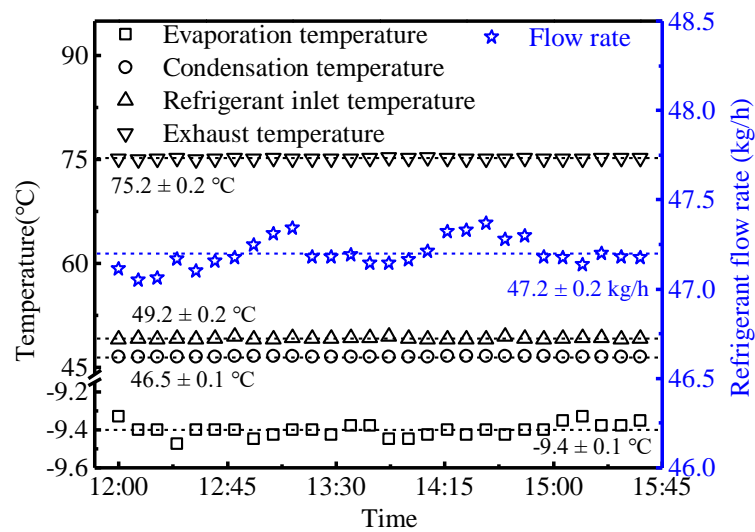


Fig. 7. Thermal characteristics of the system under the steady-state.

The heat loss of the system can be inferred from the characteristic temperatures of the system. As exhibited in Fig. 8, T_{exa} and T_{ina} are preserved at $-7\text{ }^{\circ}\text{C}$ and $18\text{ }^{\circ}\text{C}$. As T_{con} increases from $40.1\text{ }^{\circ}\text{C}$ to $55.5\text{ }^{\circ}\text{C}$, the superheat of the inlet refrigerant changes from $0.3\text{ }^{\circ}\text{C}$ to $11.2\text{ }^{\circ}\text{C}$. The heat provided by the superheat section increases from 5.9 W to 398.7 W , accounting for $0.3\% \sim 15.5\%$ of the heating capacity of the DRHP. Meanwhile, the differences between the exhaust temperature and inlet temperature change from $21.1\text{ }^{\circ}\text{C}$ to $26.0\text{ }^{\circ}\text{C}$, with an average value of $24.7\text{ }^{\circ}\text{C}$. Accordingly, the heat loss of the pipeline 2-2' increases from 401.9 W to 548.8 W , and the heat loss caused by the pipeline accounts for 18.5% of the total heat emission of the system. In practical application, the heat loss can be reduced by strengthening heat preservation and shortening connection length.

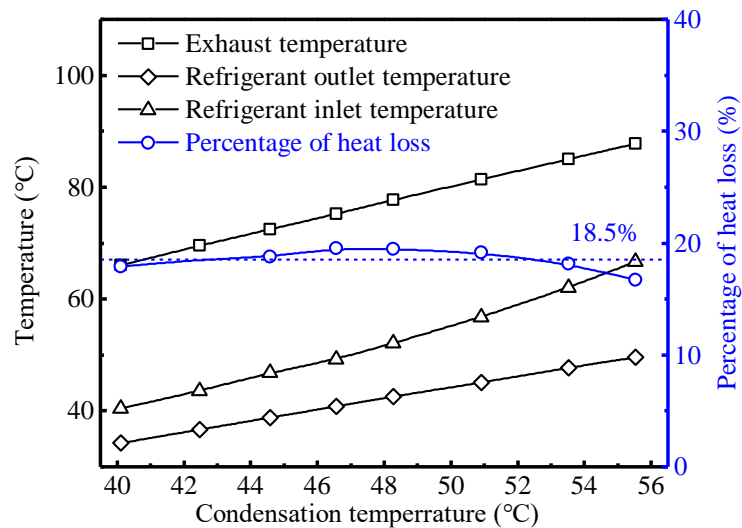


Fig. 8. Variations of the system characteristic temperatures.

4.2. Energy and exergy efficiencies of the system

The exergy destructions and efficiencies of the system in the typical heating

condition are shown in Tables. 6 and 7. The pressure P_0 of 1.013 MPa and external air temperature T_0 of $-7\text{ }^\circ\text{C}$ is taken as the dead state. Meanwhile, the reference point of the refrigerant for the enthalpy and entropy evaluation in Table. 6 is consistent with the dead state [46, 47]. Due to the degradation of useful work in the conversion of electrical energy into mechanical and thermal energy, the maximum exergy destruction occurs in the rotary compressor, accounting for 42.0% of the total exergy destruction. The exergy efficiency of the compressor is 66.7%. Meanwhile, the exergy destruction of EEV is remarkable for the heat loss caused by the conversion of refrigerant internal energy into kinetic energy. And the exergy destruction and exergy efficiency of EEV is 116.3 W and 85.4%, respectively. Based on the system thermodynamic model, the system COP and system exergy efficiency are 2.4 and 20.3% in the typical heating condition.

Besides, the influence of the external air temperature (T_{exa}), the indoor air temperature (T_{ina}) and the condensation temperature (T_{con}) on the system exergy and energy efficiency are estimated.

Table. 6. Property data of the ASHP system with the DRHP under the typical heating condition.

Number	Fluid	Position	State	Flow rate m (kg/s)	Temperature T (°C)	Pressure P (bar)	Specific enthalpy h (kJ/kg)	Specific entropy s (kJ/kg k)	Exergy rate Ex (kW)
0	R-410A	-	Reference point	-	-7.00	1.01	434.03	2.08	
1	R-410A	Evaporator outlet	Vapor	0.01311	-9.10	5.87	418.44	1.83	0.66
1'	R-410A	Compressor inlet	Vapor	0.01311	-8.85	5.87	418.70	1.83	0.66
2	R-410A	Compressor outlet	Vapor	0.01311	75.2	28.28	467.76	1.84	1.26
2'	R-410A	DRHP inlet	Vapor	0.01311	49.20	28.28	428.68	1.73	1.15
3'	R-410A	DRHP outlet	Liquid	0.01311	40.80	28.28	267.35	1.22	0.80
3''	R-410A	EEV inlet	Liquid	0.01311	40.20	28.28	266.20	1.22	0.80
4	R-410A	EEV outlet /Evaporator inlet	Mixture	0.01311	-9.40	5.87	266.20	1.25	0.68

Table. 7. Exergy destruction and exergy efficiency under the typical heating condition.

Component	EX_{in} [W]	EX_{out} [W]	EX_{dest} [W]	Φ [%]
Evaporator	678.9	661.2	17.7	97.4
Compressor	1551.2	1255.1	296.1	66.7
Condenser (DRHP)	1150.6	978.4	172.2	51.2
Expansion valve	795.2	678.9	116.3	85.4
Pipeline	1255.1	1150.6	104.5	91.7
System	5431.0	4724.3	706.7	20.3

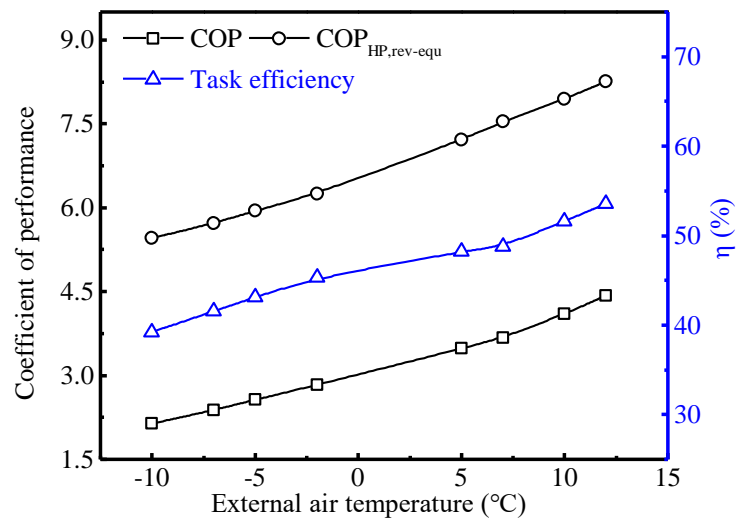
4.2.1. Effects of external air temperature

The energy and exergy performances of the ASHP system with the DRHP under different T_{exa} are displayed in Fig. 9. To investigate the effect of a single variable on the system performances, T_{con} and T_{ina} are maintained around 46.5 ± 0.4 °C and 18 ± 0.1 °C. The heating capacity of the DRHP is maintained at a certain value while the input power is reduced under the increased T_{exa} . Accordingly, the system COP and $COP_{HP,rev-equ}$ are enhanced from 2.13 to 4.37 and from 5.45 to 7.95. The task efficiency of the system is improved from 39.2% to 59.6% for the reduced compression ratio in Fig. 9 (a).

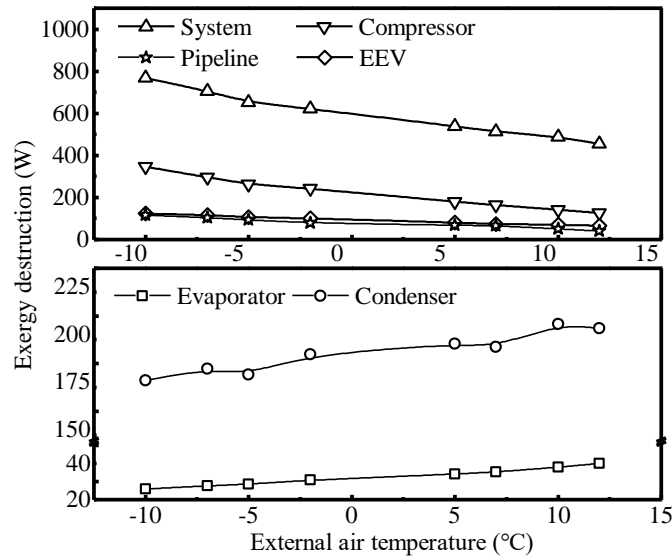
The effects of T_{exa} on system exergy destructions are exhibited in Fig. 9 (b). Owing to the declined compression ratio, the exergy destruction in the compressor, the EEV and the whole heating system is decreased with the ascendant T_{exa} . On the contrary, the exergy efficiency of the DRHP is decreased and the exergy destruction will increase from 166.1 W to 195.6 W. The phenomenon can be attributed to the decreased output exergy flow of the DRHP under the reduced temperature difference between the indoor air and external air. Meanwhile, the exergy destruction of the evaporator rises from 13.3 W to 31.9 W with the increased T_{exa} . The analogous phenomenon on the evaporator

exergy rate is also observed by Dong et al. [14] and Suleman et al. [26].

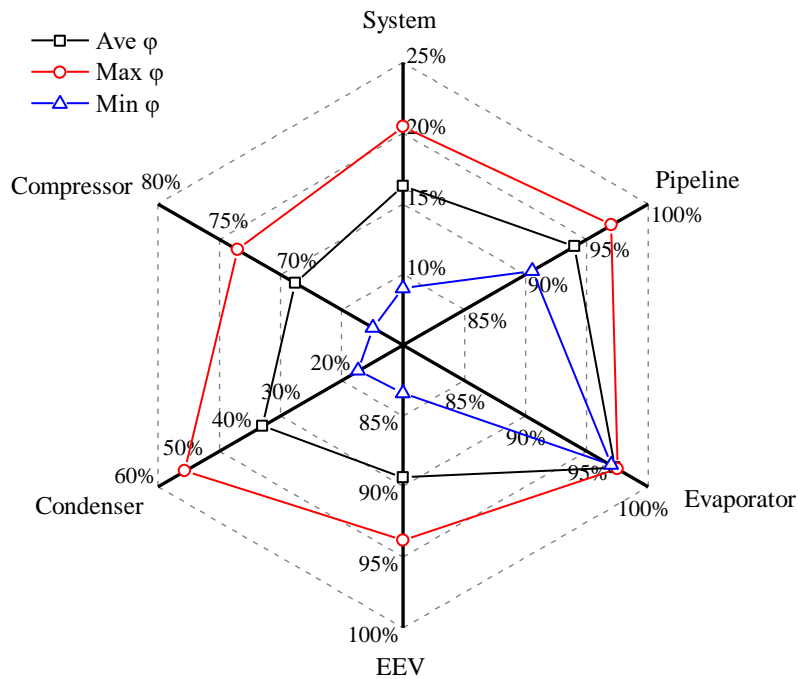
Apart from the exergy destructions, the exergy efficiencies are investigated. The variations of exergy efficiencies of system components under different T_{exa} are opposite to that of exergy destructions. Consequently, the average and extremal exergy efficiencies are analyzed, rather than the specific exergy efficiencies. As shown in Fig. 9 (c), the exergy efficiency of the evaporator is higher than 95%. This is because the refrigeration temperature difference between the inlet and outlet of the evaporator is small, and the exergy of external air is zero. In terms of the compressor and the EEV, the exergy efficiency varies from 64.2% to 74.9% and from 83.4% to 93.8% under the enhanced T_{exa} . Due to the decreased output exergy flow, the exergy efficiency of the DRHP decreases from 54.5% to 19.1% under the increased T_{exa} .



(a) Variations of COP and η under different T_{exa} .



(b) Variations of the exergy destructions under different T_{exa} .



(c) Variations of the exergy efficiencies under different T_{exa} .

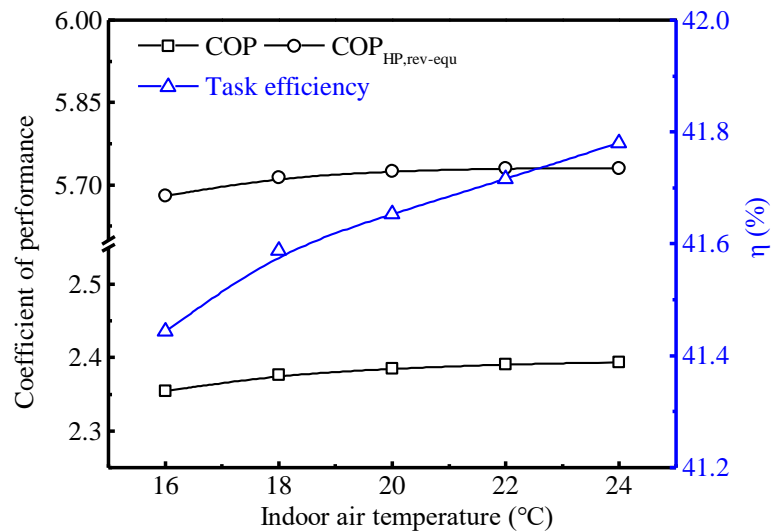
Fig. 9. Effects of external air temperature on system efficiencies.

4.2.2. Effects of indoor air temperature

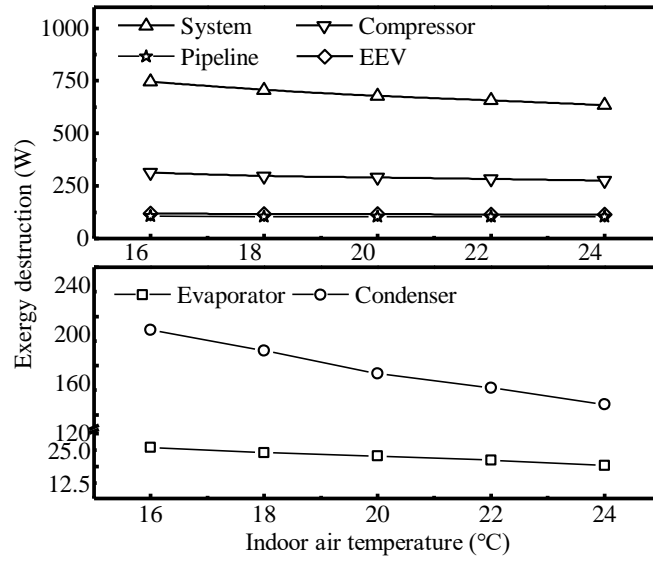
The effects of T_{ina} on system energy and exergy are displayed in Fig. 10. The T_{con} and T_{exa} are maintained around 46.5 ± 0.4 °C and -7 ± 0.1 °C in experiments. When T_{ina}

changes from 16 °C to 24 °C, the heat transfer intensity of the DRHP is inhibited, and the compressor input power is reduced under the lessened heating capacity. Correspondingly, the system COP , $COP_{HP,rev-equ}$ and the task efficiency have been improved, changing from 2.35 to 2.39, from 5.68 to 5.73, and from 41.4% to 41.8% in Fig. 10 (a).

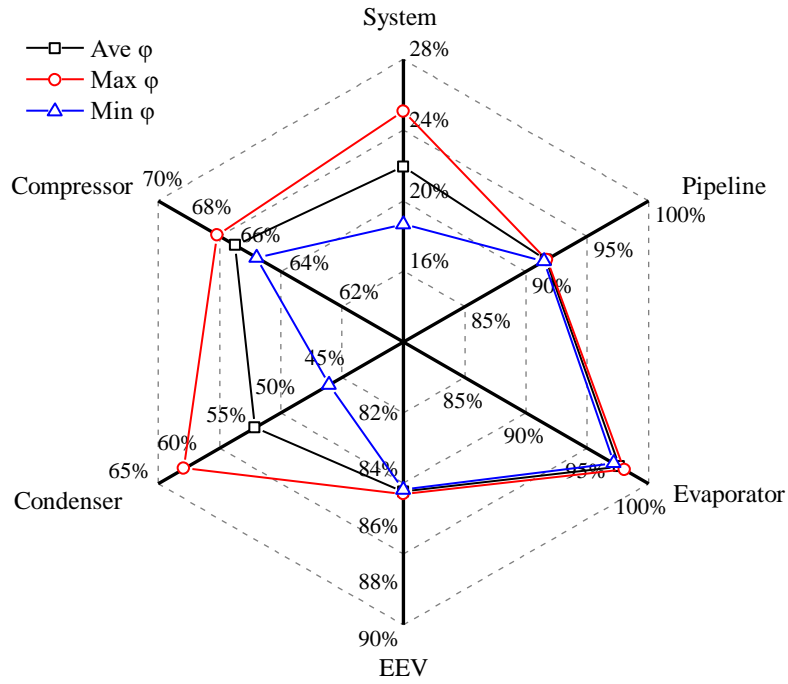
The reduced input power of the compressor contributes to the exergy efficiency of the compressor. As depicted in Fig. 10 (b) and (c), the exergy destruction of the compressor drops from 313.0 W to 275.6 W under the ascendant T_{ina} . Meanwhile, the higher T_{ina} leads to higher exergy efficiency of the DRHP, and the exergy destruction of the DRHP decreases from 188.9 W to 128.4 W in Fig. 10 (b). Nevertheless, the influences of T_{ina} on the exergy utilization of the evaporator, EEV and pipeline are negligible. The extremal exergy efficiencies of the three components preserve at 97.6%, 85.3% and 91.6% in Fig. 10 (c). The exergy efficiency of the system ranges from 18.7% to 25.1%, demonstrating that the enhanced T_{ina} is beneficial for exergy utilization.



(a) Variations of COP and η under different T_{ina} .



(b) Variations of the exergy destructions under different T_{ina} .



(c) Variations of the exergy efficiencies under different T_{ina} .

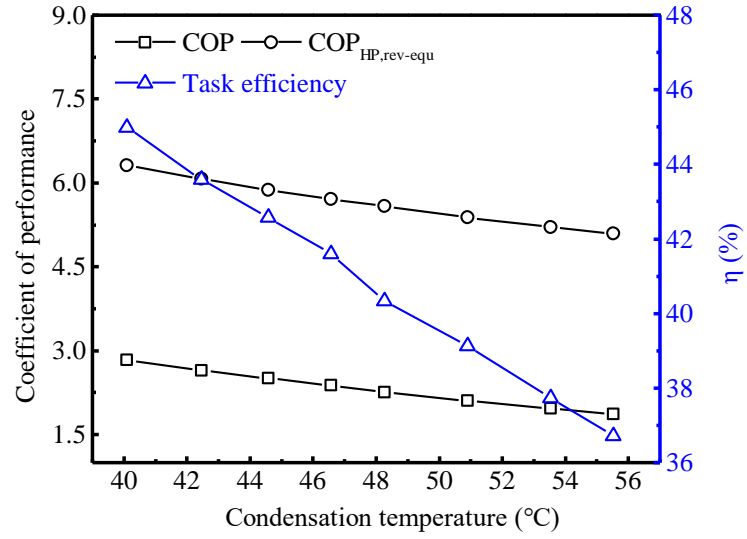
Fig. 10. Effects of indoor air temperature on system efficiencies.

4.2.3. Effects of condensation temperature

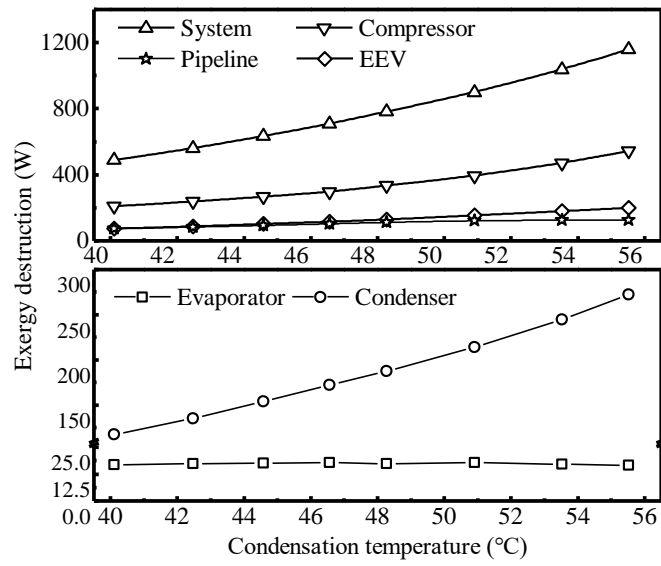
The energy rate and exergy efficiency of the system at different T_{con} are involved

in Fig. 11. The experiments are conducted at T_{exa} of -7 °C, in which T_{ina} is 18 °C, and T_{con} is stabilized at 40.5 °C, 43.0 °C, 45.1 °C, 46.5 °C, 48.8 °C, 51.4 °C, 54.0 °C and 55.7 °C, separately. The enhanced T_{con} stimulates the increased refrigerant flow rate. Accordingly, the electric power computation and the heating capacity of the DRHP are augmented. The system COP and $COP_{\text{HP,rev-equ}}$ decline from 2.84 to 1.87 and from 6.31 to 5.09 under the increased T_{con} . Meanwhile, the system task efficiency is impaired for the increased compression ratio, decreasing from 45.0% to 36.7% in Fig. 11 (a).

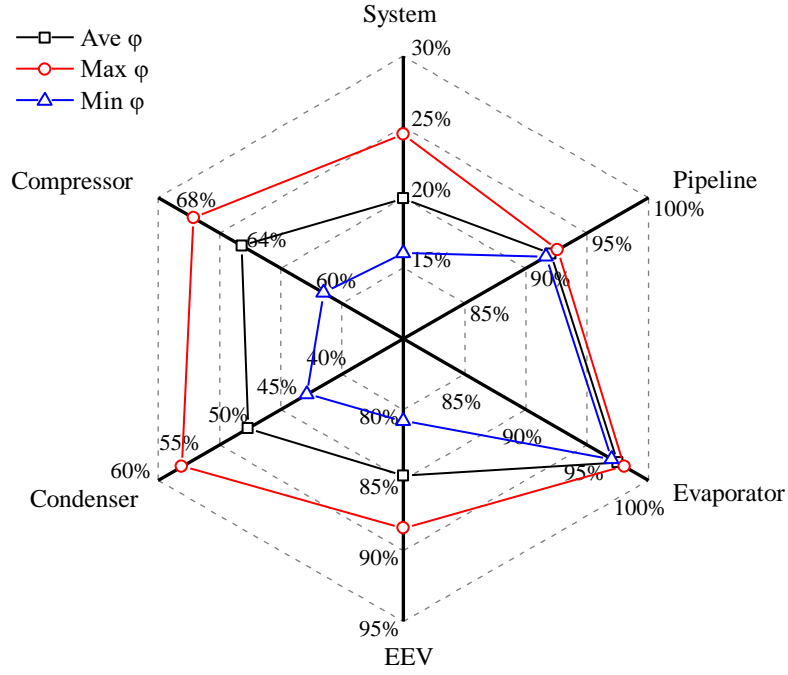
The enhanced T_{con} aggravates the system exergy destruction and impedes the system exergy utilization. As shown in Fig. 11 (b), the exergy destruction of each component is intensified in addition to the evaporator. The maximum exergy destruction occurs in the compressor, rising from 208.1 W to 544.6 W under the increased T_{con} . The slight fluctuation of the evaporator pressure is inevitable under the enhanced flow rate even if the external air temperature is controlled. Consequently, the exergy destruction in the evaporator fluctuates from 16.6 W to 17.9 W. The system exergy efficiency declines from 24.5% to 16.1% when T_{con} increases from 40.5 °C to 55.7 °C, while the exergy efficiencies of the pipeline and the evaporator are kept above 90% in Fig. 11 (c).



(a) Variations of COP and η under different T_{con} .



(b) Variations of the exergy destructions under different T_{con} .



(c) Variations of the exergy efficiencies under different T_{con} .

Fig. 11. Effects of condensation temperatures on system efficiencies.

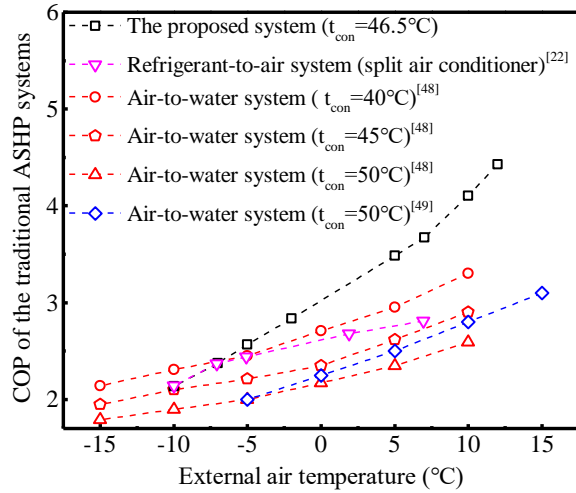
From the variations of system energy and exergy rates, it is demonstrated that the low compression ratio contributes to the system energy and exergy utilization. Moreover, the exergy efficiency of the DRHP under different operating conditions indicated that the temperature difference between indoor and outdoor environments is the major driver for the variations of the exergy efficiency.

4.2.4. Comparisons of the system efficiency

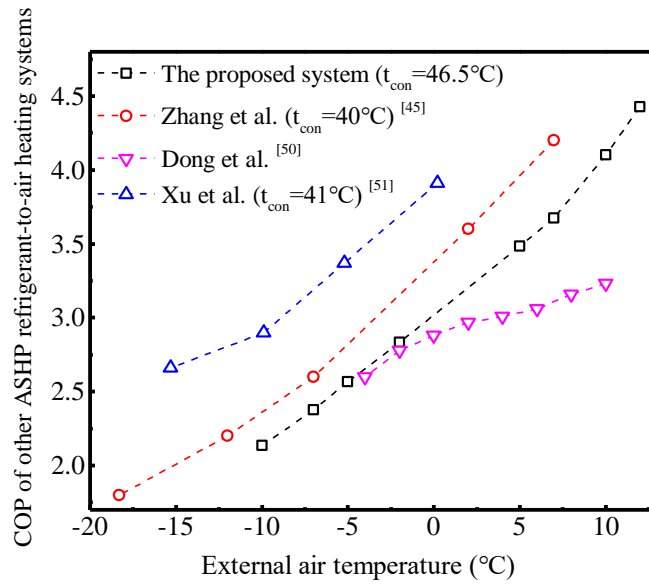
In Fig. 12, the energy efficiency of the ASHP system with DRHP is compared with other ASHP systems under the same T_{exa} and T_{con} . As shown in Fig. 12 (a), the COP of the proposed system, ranging from 2.13 to 4.41 at T_{con} of 46.5 °C, which is higher than that of the ASHP air-to-water heating system at T_{con} of 40 °C under the same T_{exa} [48]. The system performance differences between the two systems mainly originate from

the secondary heat transfer in the water heating cycle. Compared with the ASHP system with the split air conditioner, the power consumption of the indoor fan is avoided in the proposed system. Consequently, the proposed system is competitive in efficiency utilization when T_{exa} is higher than $-7\text{ }^{\circ}\text{C}$ [22].

In Fig.12 (b), the *COP* of the proposed system is compared with the ASHP system with other direct-condensation heating terminals. In Ref. 50, the system *COP* changes from 2.6 to 3.3 when T_{con} changes from $38.5\text{ }^{\circ}\text{C}$ to $45.7\text{ }^{\circ}\text{C}$, which is lower than that of the proposed system under the same heating condition. The differences between the compressors of two heat pump systems are responsible for the different *COP*. Meanwhile, the fan-less heating terminal of the proposed system contributes to reducing system input power and improving system efficiency. Compared with the efficiency in Ref. 45 and 51, the *COP* of the proposed system is lower, while it will increase when T_{con} decreases from $46.5\text{ }^{\circ}\text{C}$ to $40\text{ }^{\circ}\text{C}$. In comparison with other ASHP systems, the ASHP system with the DRHP is corroborated to be efficient and competitive, which is conducive to reducing heating energy consumption.



(a) with traditional heating terminals



(b) with other direct-condensation heating terminals

Fig. 12. Comparisons of the system *COP* with other ASHP systems

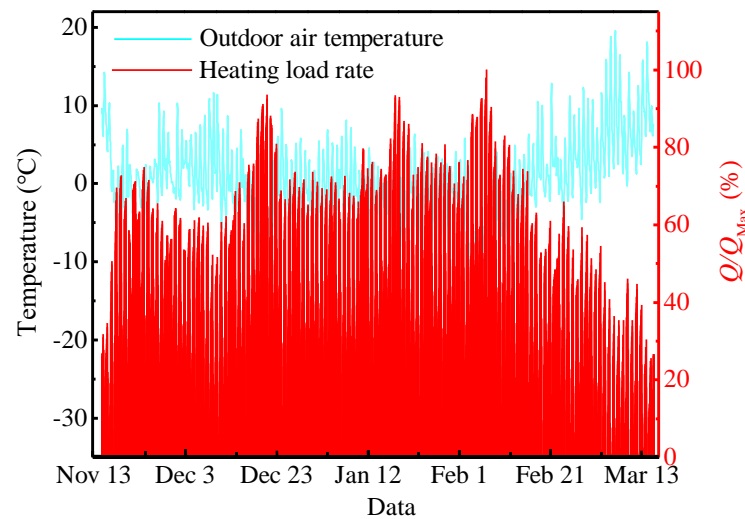
4.3. Economic evaluation of the system

The investments of each component of the ASHP system with the DRHP are categorized in Table. 8. Based on the economic model, the total C_{ICC} of the proposed system is 398.2 \$.

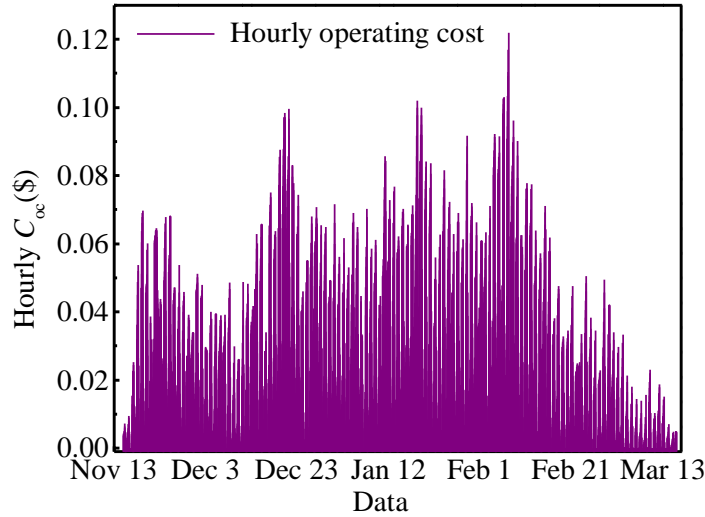
Table. 8. C_{ICC} of the proposed heating system.

Component	C_{mp} (\$)	C_{VAT} (\$)	C_{LC} (\$)
Compressor	171.3	27.4	10.5
DRHP	64.5	10.3	3.9
Evaporator	71.0	11.4	4.3
Valves & Refrigerant	19.2	3.1	1.2
C_{icc}		398.2	

To extend the application field of the system, the hourly heating load rates of the building are given rather than the specific heating load. Accordingly, the results of the case-study building could be referential for general buildings. In this paper, the hourly heating load rates of a 25 m² building are examined, and the maximum heating load is 2427.1 W in Fig. 13 (a). Details of the case-study building are provided in Appendix A. Based on the mathematical model of the system and the load rates of the case study, the total operating cost of the proposed system is 72.7 \$ in Fig. 13 (b).



(a) Hourly load rates.



(b) Hourly operating cost.

Fig. 13. Operating cost of the proposed system.

Based on C_{ICC} and C_{oc} of the proposed system, the economic indicators, such as C_{AC} , Pt , NPV and IRR of the ASHP system with DRHP are obtained, which are summarized in Table. 9. Meanwhile, the economic comparisons between the proposed system and other heating systems are also displayed in Table. 9. It should be noted that the investments of the heating systems are converted to the cost for the same heating capacity or the same heating area. As shown in Table. 9, C_{ICC} of the ASHP system with the DRHP is less than the traditional heating systems in different regions. Meanwhile, the economic indicators of the proposed system indicated that the ASHP system with the DRHP is profitable and has broad investment prospects in space heating.

Table. 9. Comparisons of the system economy with other heating systems.

Reference	Heating system	Region	Heating capacity	C_{ICC}	C_{OC}	Economic indicators
Proposed system	Refrigerant-to-air heating system with DRHP	China	3.5 kW	398.2 \$	72.7 \$	C_{AC} :139.2 \$ Pt : 7.3 year NPV : 107.4 \$ IRR : 11.2%
	Coal-fired cogeneration	China	/	410 CNY/m ² (1571.3 \$) ^a	22.1 CNY/m ²	(C_{AC} : 347.0 \$ No profit in 10 years) ^b
Zhang et al [52]	Wall hanging gas boiler heating	China	/	230 CNY/m ² (881.5 \$) ^a	13.2 CNY/m ²	(C_{AC} : 197.7 \$ No profit in 10 years) ^b
	Regional coal-fired boiler	China	/	260 CNY/m ² (996.5 \$) ^a	12.8 CNY/m ²	(C_{AC} : 215.4 \$ No profit in 10 years) ^b
Popa et al [53]	Heating boiler with liquefied petroleum gas	Romania	75 kW	6865 € (393.1 \$) ^a	30000 € per year	/
	Air-to-water heating system	Romania	75 kW	63900 € (3658.9 \$) ^a	58000 € per year	/
Ali et al [54]	Refrigerant-to-air heating system with air conditioner	Canada	9.32 kW	3086 C\$ (907.2 \$) ^a	6623 C\$ for ten years	/
Alshehri et al [55]	Refrigerant-to-air heating system with air conditioner	Saudi Arabia	38 kW	160,000 SR (3927.8 \$) ^a	6,456 SR per year	/
Li et al [56]	Refrigerant-to-air heating system with floor	China	/	160 ~170 CNY/m ² (613.2 ~ 651.5 \$) ^a	/	/

Note:

^a Figures outside the bracket () are shown in References, and figures inside the bracket () are values converted into the cost for the system with the same heating capacity or same heating area.

^b Figures inside the bracket () are values calculated with the C_{ICC} and C_{OC} .

5. Conclusions

The air source heat pump (ASHP) system with the direct-condensation radiant heating panel (DRHP) was presented and the thermal stability of the system was examined to be reliable. To evaluate the energy and exergy efficiencies of the system, a thermodynamic model was established. Meanwhile, the efficiency competitiveness of the system was demonstrated in comparison with other traditional ASHP systems. To examine the system economy, the economic model of the system was established, in which the initial cost, operating cost, and economic indicators were analyzed. In the system operating cost estimation, an effective system model was established and the hourly heating load rates of a case study were investigated. The economic competitiveness of the proposed system was validated in comparison with other heating systems. The thermo-economic model proposed in this paper contributes to the optimization and application of the ASHP system with direct-condensation heating terminals. The main conclusions are as follows:

1. The proposed system is authenticated to be reliable and effective for excellent thermal stability, and the heat loss of the pipeline accounts for 18.5% of the total heat emissions.

2. Based on the thermodynamic model, the *COP* and exergy efficiency of the proposed system are 2.4 and 20.3% in the typical heating condition. The increased indoor and external air temperature contribute to the system performance, so is the depressed condensation temperature.

4. Compared with other ASHP heating systems, the COP superiority of the ASHP system with the DRHP is demonstrated. The proposed system is conducive to reducing heating energy consumption.

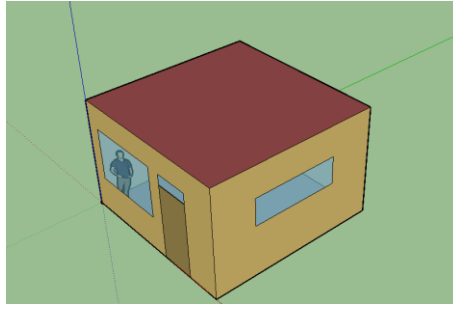
5. The mathematical model of the proposed system is corroborated to be effective for the acceptable simulation deviations. Based on the economic model, the dynamic investment pay-back period is 7.3 years, and the internal rate of return of the system is 11.2%. Compared with the traditional heating systems, the economic performances of the ASHP system with the DRHP are competitive.

Appendix A

The hourly heating load rates of the residential room model with a size of 5 m×5 m ×3.2 m (L × W× H) are examined. The structure of the case-study building is displayed in Fig. A, while the thermal characteristics of the constructions are shown in Table. A.



(a) Actual structure



(b) 3D diagram

Fig. A. The diagram of the case-study building.

Table. A. Geometry and thermal characteristics of the constructions.

Constructions	Geometry	Composition details	Heat transfer coefficients
External wall	5 m × 3.2 m	370 mm brick wall; 20 mm cement mortar; 20 mm white plaster	0.65 W/(m ² K)
East external window	2.5 m × 0.8 m	Double-pane Glass; Window frames of metal; Window curtains	2.5 W/(m ² K)
South external window	2.2 m × 0.8 m 1 m × 0.3 m	Double-pane Glass; Window frames of metal	2.8 W/(m ² K)
Door	1 m × 2 m	25 mm wooden door; Metal frame	2.5 W/(m ² K)
Floor	5 m × 5 m	35 mm concrete; 100 mm cement expanded perlite	0.6 W/(m ² K)
Roof	5 m × 5 m	35 mm concrete; 150 mm cement expanded perlite	0.5 W/(m ² K)

References

- [1] Agency International-energy. Global Energy & CO₂ Status Report: The Latest Trends in Energy and Emissions in 2018 [R]. 2018.
- [2] Agency International-energy. Global Status Report: Towards a Zero-emission, Efficient and Resilient Buildings and Construction Sector [R]. 2018.
- [3] Steve Heinen, Daniel Burke, Mark O'Malley. Electricity, gas, heat integration via residential hybrid heating technologies – An investment model assessment. *Energy*, 109 (2016), 906-919.

-
- [4] I. Staffell, D. Brett, N. Brandon, A. Hawkes. A review of domestic heat pumps. *Energy Environ*, 11 (2012), 9291–9306.
- [5] S.R. Asaee, V.I. Ugursal, I. Beausoleil-Morrison. Techno-economic feasibility evaluation of air to water heat pump retrofit in the Canadian housing stock. *Appl. Therm. Eng.*, 111 (2017), 936–949.
- [6] M. Shan, T. Yu, X. Yang. Assessment of an integrated active solar and air-source heat pump water heating system operated within a passive house in a cold climate zone. *Renewable Energy*, 87 (2016), 1059-1066.
- [7] Pei Gang, Li Guiqiang, Ji Jie. Comparative study of air-source heat pump water heater systems using the instantaneous heating and cyclic heating modes. *Applied Thermal Engineering*, 31 (2011), 342-347.
- [8] Biao Xiao, Lin He, Shihang Zhang, Tingting Kong, Bin Hu, R.Z. Wang. Comparison and analysis on air-to-air and air-to-water heat pump heating systems. *Renewable Energy*, 146 (2020), 1888-1896.
- [9] T.H. Christensen, K. Gram-Hanssen, P.E. Petersen, P. Munter, R. Marsh, T.F. Larsen, E. Gudbjerg, L.S. Rasmussen. *Varmepumper og elforbrug: Betydningen af ændrede komfortpraksisser* Danish Building Research Institute, Aalborg University, Hørsholm, Denmark (2011).
- [10] Y. Xu, Y. Huang, N. Jiang, M. Song, X. Xie, X. Xu. Experimental and theoretical study on an air-source heat pump water heater for northern China in cold winter: effects of environment temperature and switch of operating modes. *Energy Build*, 191 (2019),

164–173.

[11] Borong Lin, Zhe Wang, Hongli Sun, Yingxin Zhu, Qin Ouyang. Evaluation and Comparison of Thermal Comfort of Convective and Radiant Heating Terminals in Office Buildings. *Building and Environment*, 106 (2016), 91-102.

[12] Yinghui Wang, Xuelai Zhang, Jun ji, Zhen Tian, Yuyang Li. Numerical simulation of thermal performance of indoor airflow in heating room. *Energy Procedia*, 158 (2019), 3277–3283.

[13] Suola Shao, Huan Zhang, Lingfei Jiang, Shijun You, Wandong Zheng. Numerical Investigation and Thermal Analysis of a Refrigerant-heated Radiator Heating System coupled with Air Source Heat Pump. *Energy Procedia*, 158 (2019), 2158-2163.

[14] Xu Dong, Qi Tian, Zhen Li. Energy and exergy analysis of solar integrated air source heat pump for radiant floor heating without water. *Energy and Buildings*, 142 (2017), 128-138.

[15] K. Ma, N. Hou, X. Wang, X. Wang, Y. Gao. Analysis and study of the effect of the direct floor radiant heating system of the air source heat pump at heating working conditions. *Int. J. Simul. Syst. Sci. Technol*, 5 (2016) ,1–4.

[16] ASHRAE Standard 55. Thermal environmental conditions for human occupancy. American Society of Heating, Refrigerating and Air-Conditioning Engineers, 2004.

[17] Suola Shao, Huan Zhang, Shijun You, Wandong Zheng, Lingfei Jiang. Thermal performance analysis of a new refrigerant-heated radiator coupled with air-source heat pump heating system, *Applied Energy*, 247 (2019) 78-88.

-
- [18] Dincer I, Y.A. Cengel. Energy, entropy and exergy concepts and their roles in thermal engineering. *Entropy*, 3 (2001), 116-149.
- [19] Hideo Asada, Boelman, EC. Exergy analysis of a low temperature radiant heating system, *Building Services Engineering Research and Technology* 13(2004) 97–209.
- [20] Birol Kilkis. Exergy metrication of radiant panel heating and cooling with heat pumps. *Energy Conversion and Management*, 63 (2012), 218–224.
- [21] Radiators and Convectors–Part 2: Test Methods and Rating, (EN 442-2-2014), 2014, British Standards Institution.
- [22] JG/T 403–2013, Test Methods for Thermal Performance of Radiant Cooling and Heating Unit, Standards Press of China, Beijing, 2013.
- [23] A. Hepbasli, O. Akdemir. Energy and exergy analysis of a ground source (geothermal) heat pump system. *Energy Conversion and Management*, 45 (2004), 737-753.
- [24] M. Rahimi, S. Saedi Ardahaie, M.J. Hosseini, M. Gorzin. Energy and exergy analysis of an experimentally examined latent heat thermal energy storage system. *Renewable Energy*, 147 (2020), 1845-1860.
- [25] Ibrahim Dincer, Marc A.Rosen. Chapter 2 - Exergy and Energy Analyses. *Exergy (Second Edition) Energy, Environment and Sustainable Development*, 2013, Pages 21-30.
- [26] F. Suleman, I. Dincer, M. Agelin-Chaab. Energy and exergy analyses of an integrated solar heat pump system. *Applied Thermal Engineering*, 73 (2014), 559-566.

[27] Y. A. Çengel, M. A. Boles. Thermodynamics: An Engineering Approach. 5th edition, McGraw-Hill, 2006.

[28] Yikai Wang, Zuliang Ye, Yulong Song, Xiang Yin, Feng Cao. Energy, exergy, economic and environmental analysis of refrigerant charge in air source transcritical carbon dioxide heat pump water heater. Energy Conversion and Management, 223 (2020), 113209.

[29] Interim Regulations of the People's Republic of China on Value Added Tax, the State Council of the People's Republic of China, Beijing, 1993.

[30] Yuanlong Cui, Jie Zhu, Stamatis Zoras, YaningQiao, XinZhang. Energy performance and life cycle cost assessments of a photovoltaic/thermal assisted heat pump system[J]. Energy, 2020:118108.

[31] Fanchao Meng, Jun Guo, Guoyu Ren, LeiZhang, RuixueZhang. Impact of urban heat island on the variation of heating loads in residential and office buildings in Tianjin. Energy and Buildings, (226) 2020,110357.

[32] Wang qiankun, Hu Zhaoyi, Li Qionghui. "China's Power Tariff in the Perspective of International Comparison", Electric Power Technologic Economics, vol 21, pp 27-34, 2009, (In Chinese).

[33] Suola Shao, Huan Zhang, Wandong Zheng, ShiJun You, Yaran Wang. Numerical and experimental investigations on heat transfer performance of the refrigerant-heated radiator. Applied Thermal Engineering. (179) 2020, 115748.

[34] Jiahe Zhu, Yuying Sun, Wei Wang, Yijing Ge, Lintao Li, Jingdong Liu. A novel

Temperature-Humidity-Time defrosting control method based on a frosting map for air-source heat pumps. *International Journal of Refrigeration-Revue Internationale Du Froid*, 2015, 54: 45-54.

[35] Pongsoi P, Pikulkajorn S, Wongwises S. Heat transfer and flow characteristics of spiral fin-and-tube heat exchangers: A review. *International Journal of Heat & Mass Transfer*, 2014, 79:417-431.

[36] Meizhong S, Zhongzheng W. *Principle and design of heat exchangers*. 4th edition, Nanjing, Southeast University Press, 2009.

[37] Lopata S, Oclon P. Numerical study of the effect of fouling on local heat transfer conditions in a high-temperature fin-and-tube heat exchanger. *Energy*, 2015, 92(DEC.PT.1):100-116.

[38] Yajun Lu, Zuiliang Ma, Yang Yao. *Refrigeration technology in air conditioning engineering (Second edition)*. Harbin Engineering University Press. 2001.

[39] Sun L, Mishima K. An evaluation of prediction methods for saturated flow boiling heat transfer in mini-channels. *International Journal of Heat and Mass Transfer*. (52) 2009, 5323-5329.

[40] Liu M, Jiang L, Zhang H, et al. An exploration on the applicability of heating tower heat pump and air source heat pump Systems in different climatic regions. *Journal of Cleaner Production*, 2019, 238(Nov.20):117889.1-117889.11.

[41] Kabeel A E, Hamed A M, El-Agouz S A. Cost analysis of different solar still configurations. *Energy*, 2010, 35(7): 2901-2908.

-
- [42] Van der Tak Herman, Squire Lyn. *Economic Analysis of Projects*. 1995.
- [43] G. Ordish. *Economic Analysis of Projects*. *Outlook on Agriculture*, 1976, 9(1).
- [44] Carlos Mateu-Royoa, Joaquín Navarro-Esbría, Adrián Mota-Babilonia, Francisco Molésa,b, Marta Amat-Albuixech. Experimental exergy and energy analysis of a novel high-temperature heat pump with scroll compressor for waste heat recovery. *Applied Energy*, 253 (2019), 113504.
- [45] Huan Zhang, Lingfei Jiang, Wandong Zheng, Shijun You, Tingting Jiang, Suola Shao, Xingming Zhu. Experimental study on a novel thermal storage refrigerant-heated radiator coupled with air source heat pump heating system. *Building and Environment*. 164 (2019), 106341.
- [46] Hikmet Esena, Mustafa Inalli, Mehmet Esen, Kazim Pihtili. Energy and exergy analysis of a ground-coupled heat pump system with two horizontal ground heat exchangers. *Building and Environment* 42 (2007) 3606–3615.
- [47] Ozturk, Murat. Energy and exergy analysis of a combined ground source heat pump system. *Applied Thermal Engineering*, 2014, 73(1):362-370.
- [48] Clara Verhelst a, Filip Logist b, Jan Van Impe b, Lieve Helsen. Study of the optimal control problem formulation for modulation air-to-water heat pump. *Energy and Buildings*. 45 (2012), 43-53.
- [49] N.J. Kelly, J. Cockroft. Analysis of retrofit air source heat pump performance: Results from detailed simulations and comparison to field trial data. *Energy and Buildings*. 43 (2011), 239-245.

-
- [50] Jiankai Dong, Long Zhang, Shiming Deng, Bin Yang, Shun Huang. An experimental study on a novel radiant-convective heating system based on air source heat pump, *Energy and Buildings*, 158 (2018) 812–821.
- [51] Xu Shuxue, Ding Ruochen, Niu Jianhua, Ma Guoyuan. Investigation of air-source heat pump using heat pipes as heat radiator, *International Journal of Refrigeration*, 90, (2018) 91-98.
- [52] Qunli Zhang, Lin Zhang, Jinzhe Nie, Yinlong Li. Techno-economic analysis of air source heat pump applied for space heating in northern China, *Applied Energy* 207 (2017) 533–542.
- [53] Viorel Popa, Ion Ion, Camelia Lăcrămioara Poa. Thermo-Economic Analysis of an Air-to-Water Heat Pump, *Energy Procedia* 85 (2016) 408 – 415.
- [54] Ali Hakkaki-Fard, Parham Eslami-Nejad, Zine Aidoun, Mohamed Ouzzane. A techno-economic comparison of a direct expansion ground-source and an air-source heat pump system in Canadian cold climates, *Energy* 87 (2015) 49-59.
- [55] Faisal Alshehri, Stephen Beck, Derek Ingham, Lin Ma*, Mohammed Pourkashanian. Techno-economic analysis of ground and air source heat pumps in hot dry climates, *Journal of Building Engineering* 26 (2019).
- [56] Li Zhe, Tian Qi, Guo Wei-qiang. Research of Ventilating Performance in North China of Air-source Heat Pump Direct Radiant Floor Heating. *Science Technology and Engineering*. 14(2014), 229-232.